Quantum electron transport in toroidal carbon nanotubes with metallic leads

M. Jack* and M. Encinosa
Florida A&M University, Department of Physics, 205 Jones Hall, Tallahassee, FL 32307. *

Abstract

A recursive Green's function method is employed to calculate the density-of-states, transmission function, and current through a 150 layer (3,3) armchair nanotorus (1800 atoms) with laterally attached metallic leads as functions of relative lead angle and magnetic flux. Plateaus in the transmissivity through the torus occur over wide ranges of lead placement, accompanied by enhancements in the transmissivity through the torus as magnetic flux normal to the toroidal plane is varied.

PACS numbers: 03.65Ge, 73.22.Dj

*Corresponding author. Email: jack@cepast.famu.edu, mencinosa1@comcast.net

1. INTRODUCTION

Carbon nanotube structures and graphene materials [1, 2, 3, 4, 5, 6, 7] show promise for advancing nanoelectronics in the 21st century. Their unique mechanical, optical and electronic properties make them important materials for studying coherent quantum transport and quantum control of both charge and spin [8, 9, 10, 11, 12, 13, 14, 15, 16, 17, 18]. Toroidal carbon nanotube structures, also known as carbon nanotori, could play interesting roles in nanoelectronics, quantum computing, and as biosensors [19, 20]. To date, most of the efforts directed towards quantum rings have focused on flat two-dimensional structures [21, 22, 23, 24, 25, 26, 27, 28, 29, 30, 31, 32, 33, 34, 35, 36, 37, 38, 39]. While these objects can be more easily modelled in comparison to their toroidal counter parts, toroidal structures allow for motions around their minor radius in addition to azimuthal motion, which could give rise to novel phenomena [40, 41, 42]. Some of the potential applications by which the unique transport features of nanoscale tori might be exploited are:

- as macrosopic, three-dimensional molecular rings with persistent current effects in magnetic fields or azimuthal and dipole-type electronic excitations in microwave fields;
- as molecular Aharonov-Bohm oscillators with modulations in the current as a function of angle between the attached metallic leads or magnetic flux parallel to the toroidal symmetry axis;
- as biosensors, in which modifications of device properties are altered after covalently attaching a biopolymer.

In this paper, the density-of-states $D(E)$, transmission function $T(E)$, and current through the torus I_{SD} between two attached metallic leads under small bias are calculated via tight-binding Green's function methods. The nanotorus modelled here consists of 150 layers of a (3,3) armchair unit cell giving 1800 carbon atoms. It measures $4\mathring{A}$ in width and has a central diameter of $D = 116\mathring{A}$, making it thin compared to the graphene ring discussed in [43] where the ring width-to-radius $\frac{a}{W}$ is set to $1:5$ or $1:10$ respectively. The opening angle between the leads is varied along with magnetic flux Φ through the torus to study oscillations of I_{SD} due to constructive or destructive interference of the electronic pathways through the left and right semi-circular toroidal branches. Electron-charging effects with band-bending and modification of the Fermi-level in the torus have been shown to be small in similar small-bias device architectures utilizing carbon nanotubes, or can be sufficiently approximated with a linear potential profile in the device region without major change of results compared to the exact self-consistent treatment [44]. Thus, a full self-consistent treatment of electron-electron correlation and Coulomb repulsion effects on the quantum transport will not be discussed here. The conductivity G and I_{SD} for the small-bias case can be obtained from $T(E)$ by a convolution over E with the difference in the Fermi distributions functions $f_{L,R}$ of the left and right metallic leads [45].

This paper is organized as follows: In section 2 the Green's function formalism in the tight-binding approximation by which the results obtained here are presented. In section

3 graphs of $T(E)$ and $D(E)$ and of I_{SD} as functions of different small-bias source-drain voltages V_{SD} are shown. A magnetic field parallel to the central symmetry axis (z-axis) is applied to study I_{SD} as a function of magnetic flux through the structure. Section 4 is reserved for conclusions and suggestions for further work.

2. TRANSPORT IN THE TIGHTBINDING APPROXIMATION

The device setup for the toroidal nanotube is sketched in Figure 1. Each semi-infinite metallic leads touches the toroidal surface at four atomic contact points. The positions of these contacts can be determined from the toroidal vector $\mathbf{r}$

$$\mathbf{r}(\theta, \varphi) = (R + a\ \cos\theta)\mathbf{e}_\rho + a\ \sin\theta\mathbf{e}_z \tag{1}$$

and the relative positions of the two leads. Effectively, the curvature of the torus is neglected at the lead interface. The opening angle α between the two leads can be varied from 180^{O} (*back-to-back configuration*) down to 45^{O} (or 315^{O} respectively).

The Hamiltonian for a nanotube in the tight-binding approximation is [45]:

$$H = \sum_i E_i c_i^\dagger c_i + \sum_{i>j} \left(t_{ij} c_i^\dagger c_j + h.c. \right) \tag{2}$$

with E_i the on-site energies and the t_{ij} the hopping terms. Here all E_i=0 and the t_{ij} for the torus will be set equal to $v = -3.1\,\mathrm{eV}$ in accordance with the literature [46]. These assignments neglect any curvature effects on the t_{ij}.

The device is modelled as an open system under a small bias voltage using a Green's function method [45, 47, 48, 49]. The semi-infinite leads can be absorbed into the definition of a device Green's function G_d that serves to yield transport properties of the nanotorus. Self-energy corrections $\Sigma_{L,R}$ describing the coupling of the device region to both leads can be folded into a device Hamiltonian H_d that carries the retarded and advanced Greens functions $G_d^{(a,d)}(E)$ as solutions to a unit source via

$$\left[E - H_d - \Sigma_L - \Sigma_R \pm i\eta\right] G_d^{(a,r)} = I. \tag{3}$$

The Hamiltonian H_d is an 1800×1800 matrix at the C-C level but may be re-written as a 150×150 matrix whose elements consist of 12×12 intra or interlayer armchair coupling

submatrices A and V respectively,

$$H_d = \begin{pmatrix} A & -V^\dagger & 0 & \dots & \dots & 0 & -V \\ -V & A & -V^\dagger & 0 & \dots & 0 & 0 \\ 0 & -V & \ddots & \ddots & & & 0 \\ \vdots & 0 & \ddots & & & & \vdots \\ \vdots & \vdots & & & & \ddots & 0 \\ 0 & \vdots & & & \ddots & \ddots & -V^\dagger \\ -V^\dagger & 0 & \dots & \dots & 0 & -V & A \end{pmatrix} \tag{4}$$

A numerically fast, recursive algorithm to invert the bracketed term in Eq.(3) to compute G_d is known for an infinite nanotube. For the toroidal carbon nanotorus, however, there is an additional complication due to the corner elements in the Hamiltonian needed to achieve ring closure. An algorithm that extends the simple case to include toroidal ring closure has been developed by one of us [50]. and is employed here to determine the device Green's function. $\Sigma_{L,R}$ can be calculated analytically for semi-infinite metallic leads. All relevant transport properties can be derived from the retarded and advanced Green's functions $G_d^{(a,d)}(E)$ of the device region.

The Greens function of the semi-infinite leads, g_m, can be determined analytically. Discretizing along the longitudinal direction with lattice spacing a as is standard practice [25, 45] gives for a lead with cross-sectional area $L_y L_z$

$$g_m(E) = \frac{-8ma}{\hbar^2}\frac{1}{L_y L_z}\sum sin\frac{m\pi y}{L_y} sin\frac{n\pi z}{L_z} sin\frac{m\pi y'}{L_y} sin\frac{n\pi z'}{L_z}[\sqrt{\alpha^2{}_{mn}-1}-\alpha_{mn}], \tag{5}$$

$$\alpha_{mn} = \frac{E+E_F-E_{mn}}{t} - 1, \qquad t = \frac{\hbar^2}{ma^2}, \tag{6}$$

with E_{mn} the standard particle in a box eigenvalue expression and E_F the Fermi energy of the metal, included to account for the zero of energy being set at the tube Fermi energy $E = 0$ [45]. Eq.(5) is understood to be evaluated on the layer closest to the torus.

The exact value of the corresponding electronic coupling t_{hop} of the first atomic layer of the metallic lead surface to the torus surface is strongly dependent on the choice of the metal and its lattice structure. $t_{\text{hop}} = -0.25\,\text{eV}$ is chosen as initial default [45] and its value later modified and its effect on $T(E)$ later studied.

The formula for $D(E)$, $T(E)$ and I_{SD} under bias are summarized below. For this, the coupling terms $\Gamma_{L,R}(E)$ for the lead-torus connections are relevant and computed from the self energies $\Sigma_{L,R}$ and subsequently from $g_m(E)$:

$$\Gamma_k(E) = 2\pi i\left[\Sigma_k(E) - \Sigma_k^\dagger(E)\right] = 2\pi V_k^\dagger Im\left[g_m^k(E)\right]V_k; k = L, R. \tag{7}$$

From Eq.(3), (4) and (7), $D(E)$ and transmission $T(E)$ are determined as:

$$D(E) = G_d\left(\Gamma_L + \Gamma_R\right)G_d^\dagger; \tag{8}$$

$$T(E) = \text{Trace}\left[\Gamma_L G_d \Gamma_R G_d^\dagger\right]. \tag{9}$$

The integrated source-drain current I_{SD} is finally given as:

$$I_{SD} = \frac{2e}{h}\int_{-\infty}^{+\infty} dE\, T(E)\left[f_D\left(E-\mu_L\right) - f_D\left(E-\mu_R\right)\right] \tag{10}$$

with $f_D(E) = \frac{1}{[\exp(E-\mu)+1]}$.

Finally, we are also interested in studying coherence in electron transport induced by electrons interacting with an external magnetic field. The vector potential $\mathbf{A}(\mathbf{r})$ for a static magnetic field aligned with the toroidal symmetry axis can be written in the Coulomb gauge as:

$$\mathbf{A}(\mathbf{r}) = \frac{1}{2}B_0\rho\mathbf{e}_\varphi \rightarrow \mathbf{B} = B_0\mathbf{e}_z. \tag{11}$$

It can be shown that $\mathbf{A}(\mathbf{r})$ can be incorporated into the H_d in terms of a phase factor ζ via

$$v \rightarrow v\exp\left[\frac{ie}{\hbar}\mathbf{A}(\mathbf{r})\cdot(\mathbf{r}_i - \mathbf{r}_j)\right]. \tag{12}$$

3. RESULTS

A. Density-of-states $D(E)$ and transmission function $T(E)$

In Figure 2, density-of-states $D(E)$ and transmission function $T(E)$ plots are depicted for different choices of B_0 and t_{hop}. In Figures 2a and 2b, results for $D(E)$ and $T(E)$ are compared at $B_0 = 0$, $B_0 = 0.5\,\text{T}$ and $B_0 = 1.5\,\text{T}$. In each case the overall peak structures of $D(E)$ and $T(E)$ stay essentially unchanged. Van Hove peaks [46] are clearly enhanced with respect to the $B_0 = 0$ case. For different B_0, different peaks are enhanced. $D(E)$ has values typically in the range $\sim 10^{-2}\,\text{eV}^{-1}$ to $\sim 10^{2}\,\text{eV}^{-1}$ with enhancements up to $\sim 10^{3}\,\text{eV}^{-1}$ for energies $E = -1.0\,\text{eV}$ to $E = 1.0\,\text{eV}$. $T(E)$ ranges between $\sim 10^{-10}$ and $\sim 10^{-2}$ for the same energy interval. The symmetry of $D(E)$ and $T(E)$ for positive and negative energies is apparent. The hopping parameters at the metal-torus contacts and in the device region were set to $t_{\text{hop}} = -0.25\,\text{eV}$ and $v = -3.1\,\text{eV}$. The Fermi level in metallic leads is chosen at $E_{\text{fermi}} = 6.0\,\text{eV}$ in rough accordance with physical values.

Part (c) clearly demonstrates that improving the electronic coupling to the metallic contacts causes an increase in number of available states at the contacts into and out of which electrons can be scattered from and/or into the device region, as evidenced by a positive shift of the density-of-states $D(E)$ with an increase in t_{hop}. t_{hop} is modified here from the default value $t_{\text{hop}} = -0.25\,\text{eV}$ to $t_{\text{hop}} = -0.5\,\text{eV}$ and $t_{\text{hop}} = -1.5\,\text{eV}$ respectively. Again, values for $D(E)$ are in the range $\sim 10^{-2}\ldots 10^{3}\,\text{eV}^{-1}$. Similarly, an overall symmetric increase in $T(E)$ is observed in Figure 2d when increasing t_{hop} allowing close to unit $T(E) \approx 1$, for certain energies.

B. Coherence in electronic transmission

Up to now, results for $D(E)$ and $T(E)$ have been presented with the metallic leads attached in a *back-to-back* configuration, i.e. the opening angle α is chosen as 180^{O}. Having in mind analogous phenomena seen in flat annular structures, the question as to whether the torus could act as a macro-molecular Aharonov-Bohm oscillator arises. When changing the opening angle α between the leads and applying a bias voltage across leads, the effective path length of electrons moving in the left or right branch of the nanotorus from metallic lead to lead will differ, opening up possible interference effects between the left and right electron wave functions. Due to the quasi-ballistic nature of transport in carbon nanotube-like structures, coherence in transmission through the nanotorus should be expected. The three-dimensional geometry of the nanotorus and its finite (non-zero) width will show a modulation in the oscillations of $T(E)$ for different α observed in rings [21, 22, 23, 24, 26, 27, 28, 29, 30, 31, 32, 33, 34, 35, 36, 37, 38, 39] due to differing possible electronic pathways with different major radii varying between $R-a$ and $R+a$ in the toroidal geometry.

The recursive algorithm employed here easily allows for the modelling of a rotation of the position of one of the leads with respect to the other by determining the new positions of the four atomic contact positions for the rotated lead while the positions of the contact sites at the other fixed lead remain unchanged. A quick back-of-the-envelope estimate helps to determine the electron momenta k and thus for which de Broglie wavelengths $\lambda = \frac{2\pi}{k}$ coherence in electronic transmission is visible before the finite size of the lattice constant of the underlying graphene lattice of $a = 1.4\mathring{A}$ washes out any interference effects for higher momenta. The electronic energy E is roughly given by $E = \frac{\hbar^2 k^2}{2m_e}$. Assuming $E \approx 0.01$eV, calculate the occurence of interference minima in transmission in steps of $\Delta\alpha$ where destructive interference occurs for pathlength differences $\Delta s = (2n+1)\,\frac{\lambda}{2}$ with $n = 0, 1, 2, \ldots$ between the left and right toroidal branch:

$$\left.\begin{array}{rcl} E & \approx & 0.01\,\mathrm{eV} = \frac{\hbar^2 k^2}{2m_e} \rightarrow \lambda \approx 12.3\,\mathrm{nm} \\ R & = & 5.8\mathrm{nm} \rightarrow u = 2\pi R = 36.4\,\mathrm{nm} \end{array}\right\} \rightarrow \Delta\alpha \approx 360^{\mathrm{O}} \cdot \frac{\lambda/2}{u} = 60.6^{\mathrm{O}}. \qquad (13)$$

The minimum angular difference at which the finite lattice size starts playing a role for a (3,3) armchair carbon nanotorus with 1800 atomic sites and for the dimensions used here is $\Delta\alpha = \frac{360^{\mathrm{O}}}{150} = 2.4^{\mathrm{O}}$. Thus, for electronic energies E of ~ 0.1eV and larger, any coherence effects visible at lower energies will become negligible.

The above predicted plateaus in $T(E)$ due to constructive interference in transmission through the torus can be clearly deduced from Figures 3a and 3b. $T(E)$ was calculated for $E = 0.01\,\mathrm{eV}$ and $E = 0.02\,\mathrm{eV}$ where plateaus according to Eq.(13) were predicted. The figures show several interference curves for an angular range of $\Delta\alpha = 45^{\mathrm{O}}, \ldots, 315^{\mathrm{O}}$. At larger energies, calculations show a gradual flattening of the plateaus and eventually a disappearance of coherence effects at $E = 0.1\,\mathrm{eV}$ and $E = 0.2\,\mathrm{eV}$ respectively. At smaller energies on the order of 0.001eV or less, $T(E)$ appears essentially flat with small amplitudes $\sim 10^{-4}$ and less, quickly decreasing when turning on and increasing B_0. B-field values from

0 T to larger fields of 5.0 T have been chosen to determine any dependence of the position of the plateaus as a function of flux threading the nanotorus plane. A substantial enhancement of $T(E)$ by about one order of magnitude occurs for specific B_0 values $B_0 \approx 1.0 \ldots 1.5\,\mathrm{T}$; the exact B-field for maximum $T(E)$ plateau shifts to larger values with increasing energy E.

For comparison, the $T(E)$ plots for non-resonant magnetic field values are shown enhanced in the insets. The resonant B-field dependence of the transmission plateaus at the higher scale corresponds to the internal atomic scale of the torus, $a = 1.4\mathring{A}$. In this case, the magnetic phase $\zeta = e^{i\Phi/\Phi_0}$ with $\Phi_0 = \frac{h}{e}$ creates a B-field dependent electronic interference on top of the previously discussed interference effect due to different opening angles α. In simple terms, constructive and destructive interferences are generated by a magnetic phase change ζ that accrue from lattice site to lattice site along the toroidal circumference to yield overall macroscopic phase changes for coherence in transmission from the left and right toroidal branches while at the larger scale this macroscopic phase change already occurs for electron hopping from lattice site to adjacent lattice site. Further details can be found in Subsection 3.3.

C. I_{SD} with magnetic flux; the torus as an Aharonov-Bohm oscillator

Under a small voltage bias V_{SD}, I_{SD} can be determined from Eq.(10) by an integration over the transmission function $T(E)$ convolved with the difference in the Fermi distributions of the two metallic leads. (Here the effect of the field on the leads has been neglected but should be considered in more comprehensive work.) I_{SD} is plotted as a function of V_{SD} in Figures 4a and 4c for a number of different B_0 while Figures 4b and 4d show the dependency of I_{SD} on Φ for two V_{SD} values.

Linear voltage-current profiles for the small-bias case can be clearly shown in Figures 4a and 4c for back-to-back leads and 90^{O} lead opening angle. The slope of the curves yields the conductance $G \times V_{SD}$ with G as conductivity as predicted from Landauer-Büttiker theory in small-bias approximation [51, 52]. The current can change by a factor of roughly 2.5 when choosing $B_0 = 0, 0.5, 1.0, 1.5, 2.0\mathrm{T}$. From this depiction no pattern in the dependency of I_{SD} on B_0 can be detected.

Following the discussion of coherence patterns in transmission for different opening angles between leads, one could conceive of achieving similar interference effects by increasing magnetic flux $\Phi = \int\limits_c \mathbf{A}\, d\mathbf{r}$ through the torus. The flux ratio $\frac{\Phi}{\Phi_0}$ with respect to Φ_0 can be equated with a magnetic field ratio $\frac{B}{B_0}$ with $B_0 = 0.026\,\mathrm{T}$. The current I_{SD} is plotted here as a function of the flux ratio $\frac{\Phi}{\Phi_0}$. For both the 180^{O} and 90^{O} lead configurations, similar oscillations of I_{SD} with changing magnetic flux are demonstrated. In each case, the strongly oscillatory curve appears to be composed of a superposition of two simpler oscillations in Φ not shown here with Φ as even or odd multiples of $\frac{1}{16}\Phi_0$. Constructive and destructive interference in electronic transmission can thus be generated due to phase angle difference

with magnetic fluxes at the scale of $\frac{\Phi_0}{16}$. The flux period of these oscillations can be read off from the plots as $\Delta\Phi = \frac{3}{16}\Phi_0$. For comparison, magnetic flux dependencies are mainly computed and shown in the literature for persistent currents for two- and three-dimensional ring geometries [32, 33, 34, 43], but the magnitude of I_{SD} for example is comparable to the current magnitude expected in a two-dimensional graphene ring under similar conditions when re-scaling the results in [43] to the torus dimensions here. Also, the general oscillatory behavior with changing magnetic flux appears to agree with findings reported there and other places [22, 23, 24, 26, 27, 28, 29, 30, 31, 32, 33, 34, 35, 36, 37, 38, 39].

To compute $I_{SD}\,(V_{SD})$, $T(E)$ is calculated symmetrically around the device Fermi level E_f^d between the energies $E = -0.2$eV and $E = 0.2$eV for a step size of 5×10^{-5}eV where E_f^d has been set to zero. $T(E)$ is then integrated over this energy region with the difference in Fermi distributions according to Eq.(10) to approximately yield I_{SD}. For the small-bias case $V_{SD} = 0, \ldots, 0.1$eV, contributions to the energy integration of I_{SD} beyond the chosen energy range may be safely neglected due to the fast exponential drop-off of the Fermi functions.

4. CONCLUSIONS

The authors employ a recursive Green's function algorithm to calculate the electronic density-of-states $D(E)$ and transmission functions $T(E)$ of a thin toroidal carbon nanotube under a small bias voltage between laterally attached metallic leads.

A strong enhancement of $D(E)$ and $T(E)$ is observed when the nanotorus is threaded with a magnetic flux Φ, particularly near van Hove peaks [46]. The enhancement is pronounced with increasing magnetic field. An increase of the hopping parameter t_{hop}, which governs the effective electronic coupling at the metal-nanotorus atomic contact sites, also shifts $D(E)$ and $T(E)$ for all energies.

Coherent electronic interference phenomena could be observed in $T(E)$ as a function of the angle α between the metallic leads, and in the integrated source-drain current I_{SD} as a function of magnetic flux. $T(E)$ shows clear maximum and minimum plateaus for specific angular ranges where constructive or destructive interference of the electronic wave functions for electrons moving left or right in the torus from one lead to the other can be expected depending on the opening angle α. Due to finite size effects in the nanotorus (i.e. the torus has a non-zero width) the constructive interference regions are broadened to plateaus over a range of angles and not simply peak-like maxima. Similarly, constructive and destructive electron interference appears in I_{SD} when applying B_0 where effective path length differences are induced by a magnetic phase angle $e^{i\Phi/\Phi_0}$, different for the left and right toroidal branches. I_{SD} measured in units of $\frac{e}{h}$ shows strong oscillations in Φ/Φ_0. The magnitude of I_{SD} is comparable to the current expected in a two-dimensional graphene ring under similar conditions after re-scaling the results in [43] to the toroidal dimensions.

Natural extensions of the model and methods of this work are towards larger systems with more than tens of thousands of carbon atoms, and to include nearest and next-to-nearest neighbor contributions. For flat two-dimensional graphene nanoribbons, an opening of an

energy bandgap has been predicted [18]. Similar effects can be expected to appear in an expanded calculation for the three-dimensional geometries. Furthermore, a more realistic device setup with the metallic leads attached at the 'bottom' of the torus, i.e. the torus lieing flat on the two planar leads will allow an increase in the number of metal-carbon contact sites and possibly lead to better and closer lead attachment. This could prove to be very interesting in the context of an applied microwave field with an additionally tilted static magnetic field due to the interplay between electronic excitations and persistent and bias-driven currents through the torus [40, 41, 42]. It is conceivable that quantum control applications could follow when the induced dipole and solenoidal magnetic moments couple to electronic spin.

Acknowledgments

One of the authors (M.E.) would like to thank M.P. Anantram and M. Meyyapan for initially suggesting this project and for helpful support by the NASA Ames Research Center. M.J. is currently being supported under NSF Grant 0603070. Both authors would also like to thank L. Johnson and N. Christopher at Florida A&M University's Laser Remote Sensing Laboratory (LRSL) Computer Cluster.

---

[1] S. Iijima. Helical microtubules of graphitic carbon. *Nature (London),* **354**, 56 (1991).

[2] K.S. Novoselov, A.K. Geim, S.V. Morozov, D. Jiang, Y. Zhang, I.V. Gigorieva, S.V. Dubonos, A.A. Firsov. Electric Field Effect in Atomically Thin Carbon Films. *Science,* **306**, 666 (2004).

[3] K.S. Novoselov, D. Jiang, F. Schedlin, T.J. Booth, V.V. Khotkevich, S.V. Morozov, A.K. Geim. Two Dimensional Atomic Crystals. *Proc. Natl. Acad. Sci. USA,* **102**, 10451 (2005).

[4] K.S. Novoselov, A.K. Geim, S.V. Morozov, D. Jiang, M.I. Katsnelson, I.V. Gigorieva, S.V. Dubonos, A.A. Firsov. Two-Dimensional Gas of Massless Dirac Fermions in Graphene. *Nature (London),* **438**, 197 (2005).

[5] Y. Zhang, Y. Tan, H. L. Störmer, P. Kim. Visibility of graphene flakes on a dielectric substrate. *Nature (London),* **438**, 201 (2005).

[6] N.M.R. Peres, F. Guinea, A.H. Castro Neto. Electronic Properties of Disordered Two-Dimensional Carbon. *Phys. Rev. B,* **73**, 125411 (2006).

[7] V.M. Pereira, F. Guinea, J.M.B. Lopes dos Santos, N.M.R. Peres, A.H. Castro Neto. Disorder Induced Localized States in Graphene. *Phys. Rev. Lett.,* **96**, 036801 (2006).

[8] M. Shapiro, P. Brumer (Eds.). *Principles of the quantum control of molecular processes,* John Wiley & Sons, Hoboken, NJ, (2003).

[9] A. Borzi, G. Stadler, U. Hohenester. Optimal quantum control in nanostructures: Theory and application to a generic three-level system. *Phys. Rev. A,* **66**, 053811 (2002).

[10] W. Potz. Coherent control of terahertz radiation from semiconductor nanostructures. *Appl. Phys. Lett.,* **72**, 3002 (1998).

[11] H. Qin, D. W. van der Weide, J. Truitt, K. Eberl, R. H. Blick. Electron dynamics of an artificial atom probed by pulsed microwave spectroscopy. *Nano. Lett.,* **14**, 60 (2003).

[12] T. H. Oosterkamp, T. Fujisawa, W. G. van der Weil, K Ishibashi, R. V. Hijman, S. Tarucha, L. P. Kouwenhoven. Microwave spectroscopy of a quantum-dot molecule. *Nature,* **395**, 873 (1998).

[13] B. Trauzettel, D.V. Bulaev, D. Loss, G. Burkard. Spin qubits in graphene quantum dot. *Nature Physics,* **3**, 192 (2007).

[14] A. Rycerz, J. Tworzydlo, C.W.J. Beenakker. Valley filter and valley valve in graphene. *Nature Physics,* **3**, 172 (2007).

[15] E.W. Hill, A.K. Geim, K.S. Novoselov, F. Schedin, P. Blake. Graphene Spin Valve Devices. E-print archive: cond-mat.mes-hall/0704.3165.

[16] Y.-W. Son, M.L. Cohen, S.G. Louie. Half-metallic graphene nanoribbons. *Nature,* **444**, 347 (2006).

[17] Y.-W. Son, M.L. Cohen, S.G. Louie. Half-metallic graphene nanoribbons. *Nature (Corrigendum),* **446**, 347 (2007).

[18] Y.-W. Son, J. Ihm, M.L. Cohen, S.G. Louie, H.J. Choi. Electrical switching in metallic carbon nanotubes. *Phys. Rev. Lett.,* **95**, 216602 (2005).

[19] B.R. Goldsmith, J.G. Coroneus, V.R. Khalap, A.A. Kane, G.A. Weiss, P.G. Collins. Conductance-Controlled Point Functionalization of Single-Walled Carbon Nanotubes. *Science,* **315**, 77 (2007).

[20] J. Mannik, B.R. Goldsmith, A. Kane, P.G. Collins. Chemically induced conductance switching in carbon nanotube circuits. *Phys. Rev. Lett.,* **97**, 016601 (2006).

[21] L. Liu, G.Y. Guo, C.S. Jayanthi, S.Y. Wu. Electrical conductance of carbon nanotori in contact with single-wall carbon nanotubes. *Phys. Rev. Lett.,* **88**, 217206-1 (2002).

[22] D.V. Bulaev, V.A. Geyler, V.A. Margulis. Effect of the surface curvature on the magnetic moment and persistent currents in two-dimensional quantum rings and dots. *Phys. B,* **69**, 195313 (2004).

[23] J. I. Climente, J. Planelles, F. Rajadell. Energy structure and far-infrared spectroscopy of two electrons in a self-assembled quantum ring. *J. Phys. Cond. Matt.,* **17**, 1573 (2005).

[24] W. Tian, S. Datta. Aharonov-Bohm-type effect in graphene tubules: A Landauer approach. *Phys. Rev. B,* **49**, 5097 (1994).

[25] S. Datta (Ed.). *Electronic Transport in Mesoscopic Systems,* Cambridge Univ. Press, Cambridge, MA (1995).

[26] I. Filikhin, E. Deyneka, B. Vlahovic. Energy dependent effective mass model of InAs/GaAs quantum ring. *Modelling Simul. Mater. Sci. Eng.,* **12**, 1121 (2004).

[27] A. Fuhrer, S. Lüscher, T. Ihn, T. Heinzel, K. Ensslin, W. Wegscheider, M. Bichler. Energy spectra of quantum rings. *Nature,* **413**, 822 (2001).

[28] L. Georgiev, M. Geller. Magnetic Moment Oscillations in a Quantum Hall Ring. *Phys. Rev. B,* **70**, 155304 (2004).

[29] S. Gylfadottir, M. Nita, V. Gudmundsson, A. Manolescu. Net current generation in a 1D quantum ring at zero magnetic field. *Phys. E,* **27**, 209 (2005).

[30] A.I. Ivanov, O.R. Lobanova. Magnetic field effects on circular cylinder quantum dots. *Phys. E,* **23** , 61 (2003).

[31] S. Latil, S. Roche, A. Rubio. Persistent currents in carbon nanotube based rings. *Phys. Rev. B,* **67,** 165420 (2003).

[32] Y.V. Pershin, C. Piermarocchi. Laser-controlled local magnetic field with semiconductor quantum rings. *Phys. Rev. B,* **72**, 245331 (2005).

[33] Y.V. Pershin, C. Piermarocchi. Persistent and radiation-induced currents in distorted quantum rings. *Phys. Rev. B,* **72**, 125348 (2005).

[34] K. Sasaki, Y. Kawazoe, R. Saito. Aharonov-Bohm effect in higher genus materials. *Phys. Lett. A,* **321**, 369 (2004).

[35] K. Sasaki, Y. Kawazoe. Characteristic Behavior of Toroidal Carbon Nanotubes: Kinematics of Persistent Currents. *Prog. Theo. Phys.,* **112**, 369 (2004).

[36] J. Simonin, C.R. Proetto, Z. Barticevic, G. Fuster. Single-particle electronic spectra of quantum rings: A comparative study. *Phys. Rev. B,* **70**, 205305 (2004).

[37] S. Viefers, P. Koskinen, P. Singha Deo, M. Manninen. Quantum rings for beginners: Energy spectra and persistent currents. *Phys. E,* **21**, 1 (2004).

[38] S.K. Maiti. Electron transport through mesoscopic ring. *Phys. E,* **36**, 199 (2007).

[39] E. Papp, C. Micu, L. Aur, D. Racolta. Period doubling effects in the oscillations of persistent currents in discretized AharonovBohm rings. *Phys. E,* **36**, 178 (2007).

[40] M. Encinosa, M. Jack. Elliptical tori in a constant magnetic field. *Phys. Scr.,* **73**, 439 (2006).

[41] M. Encinosa, M. Jack. Dipole and solenoidal magnetic moments of electronic surface currents on toroidal nanostructures. Journal of Computer-Aided Materials Design (Springer), May (2006). Proceedings of the Conference Synergy between Experiment and Computation in Nanoscale Science at Harvard Universitys Center for Nanoscale Systems, Cambridge, MA, May 31 June 3 (2006).

[42] M. Encinosa, M. Jack. Excitation of surface dipole and solenoidal modes on toroidal structures. E-print archive: physics/0604214.

[43] P. Recher, B. Trauzettel, Ya.M. Blanter, C.W.J. Beenakker, A.F. Morpurgo. Aharonov-Bohm effect and broken valley-degeneracy in a graphene ring, E-print archive: cond-mat.mes-hall/07062103.

[44] Y. Xue, S. Datta, M. Ratner. First-principles based matrix Green's function approach to molecular electronic devices: General formalism. *Chem. Phys.,* **281**, 151 (2002).

[45] M.P. Anantram, T.R. Govindan. Conductance of carbon nanotubes with disorder: A numerical study. *Phys. Rev. B,* **58**, 4882 (1998).

[46] M.S. Dresselhaus, G. Dresselhaus, P.C. Eklund (Eds.). *Science of Fullerenes and Carbon Nanotubes,* Academic Press, New York, (1996).

[47] C. Caroli, R. Combescot, P. Nozieres, D. Saint-James. Direct calculation of the tunneling current. *J. Phys. C,* **4**, 916 (1971).

[48] Y. Meir, N.S. Wingreen. Landauer formula for the current through an interacting electron region. *Phys. Rev. Lett.,* **68**, 2512 (1992).

[49] J.-C. Charlier, T.W. Ebbesen, Ph. Lambin. Structural and electronic properties of pentagon-heptagon pair defects in carbon nanotubes. *Phys. Rev. B,* **53**, 11108 (1996).

[50] M. Encinosa. Unpublished results.

[51] R. Landauer. Shot noise in mesoscopic systems. *IBM J. Res. Dev.,* **1**, 1957 (1957).

[52] M. Büttiker. Four-Terminal Phase-Coherent Conductance. *Phys. Rev. Lett.,* **57**, 1761 (1986).

Figure captions

Figure 1. Sketch of device setup with toroidal carbon nanotube and metallic leads.

Figure 2. *Density-of-states $D(E)$ and transmission function $T(E)$ as a function of energy E:* a. $D(E)$ for different magnetic fields B_0. b. $T(E)$ for different magnetic fields B_0. c. $D(E)$ for different electronic coupling terms $t_{\rm hop}$ between torus and metallic leads. d. $T(E)$ for different hopping terms $t_{\rm hop}$.

Figure 3. *Coherence in electronic transport. Plateaus in electronic transmission:* a. Transmission function $T(E)$ at $E = 0.01\,\mathrm{eV}$ as a function of magnetic field B for different angles α between metallic leads. b. Transmission function $T(E)$ at $E = 0.02\,\mathrm{eV}$.

Figure 4. *Back-to-back leads:* a. Source-drain current I_{SD} as a function of source-drain voltage $V_{SD}[\,\mathrm{eV}]$ (small bias) for different magnetic fields B_0. I_{SD} in units of $\frac{e}{h}$. Chemical potential at left/right lead: $\mu_{1,2} = \pm\frac{V_{SD}}{2}$. Thermal energy: $k_BT = 30\,\mathrm{meV}$. b. Source-drain current I_{SD} as a function of applied magnetic field $B_0[\,\mathrm{T}]$ ($V_{SD} = 0.1\,\mathrm{eV}$). 90^o *angle btw. leads:* c. Source-drain current I_{SD}versus source-drain voltage $V_{SD}[\,\mathrm{eV}]$. d. Source-drain current I_{SD} versus magnetic field $B_0[\,\mathrm{T}]$.

Figures

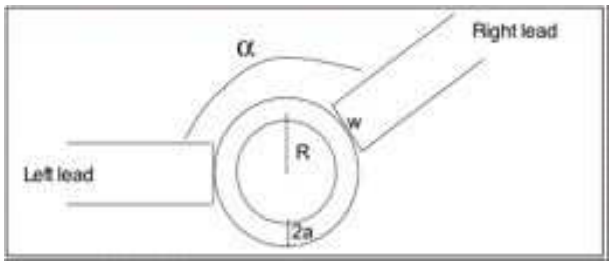

Fig. 1.

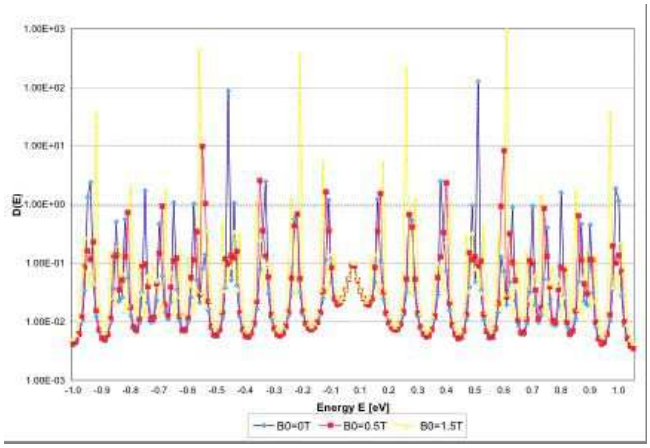

Fig. 2 a.

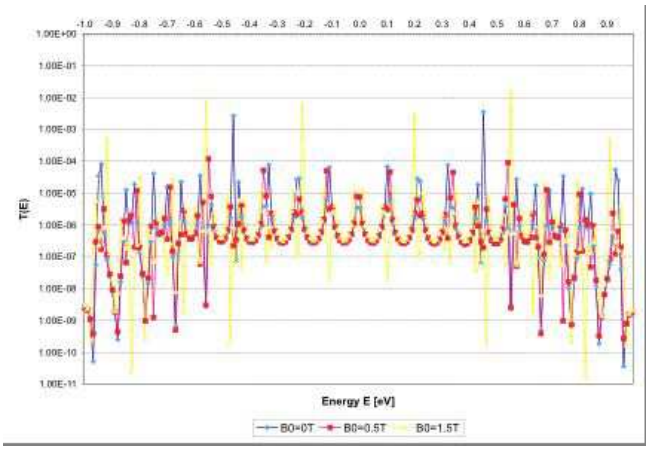

Fig. 2 b.

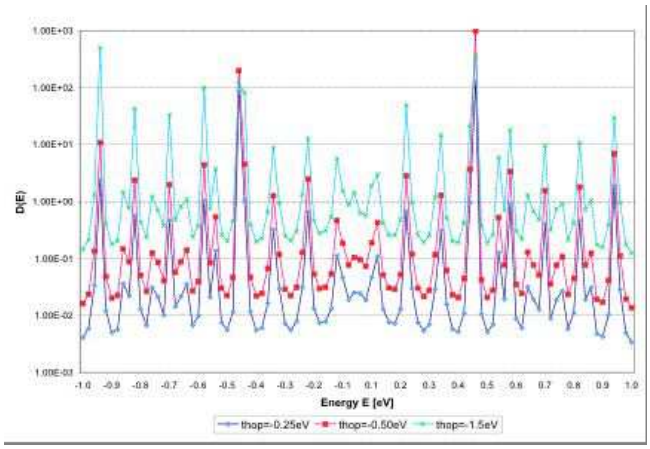

Fig. 2 c.

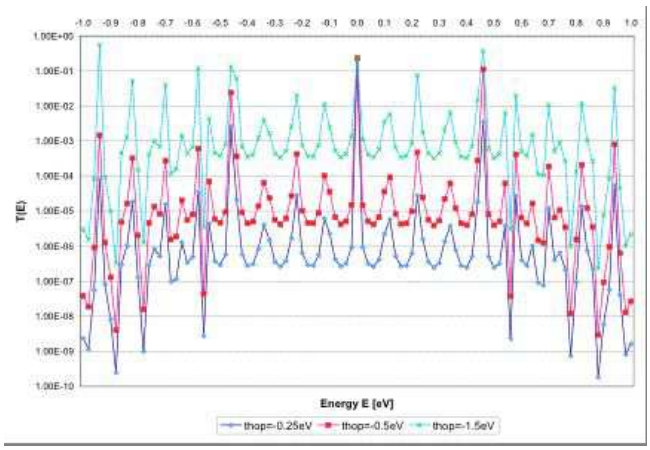

Fig. 2 d.

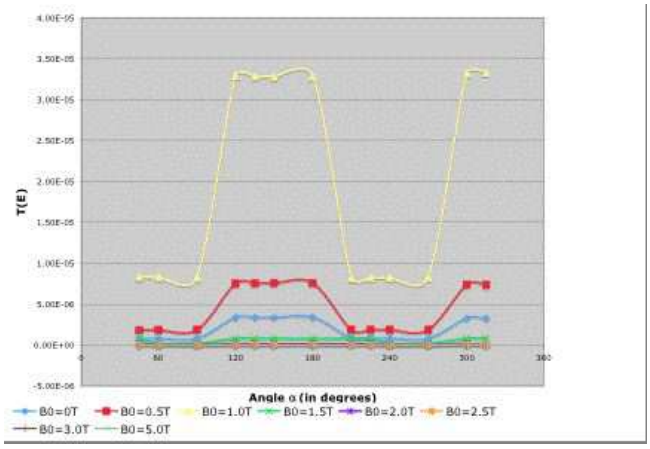

Fig. 3 a.

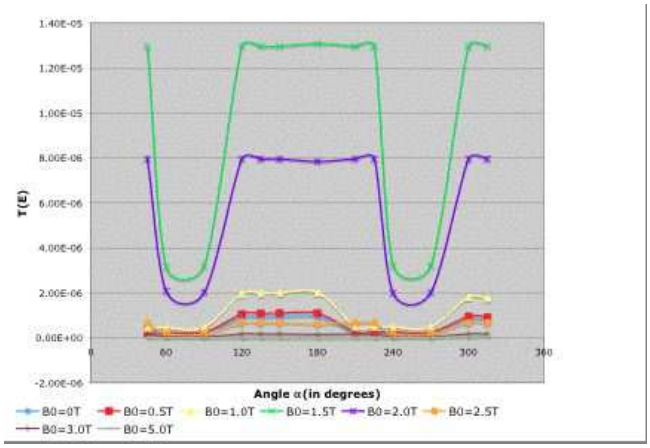

Fig. 3 b.

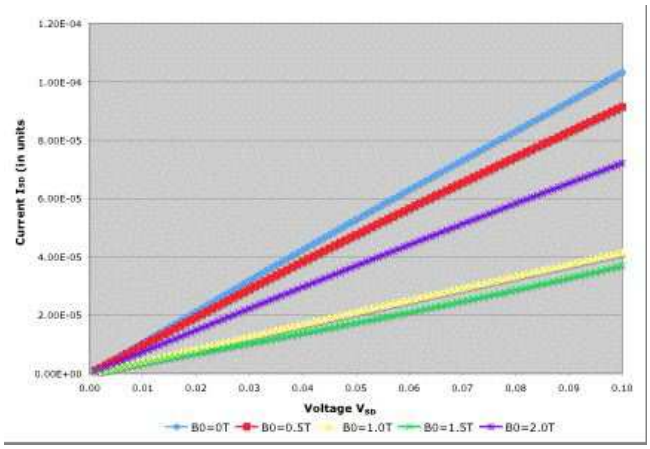

Fig. 4 a.

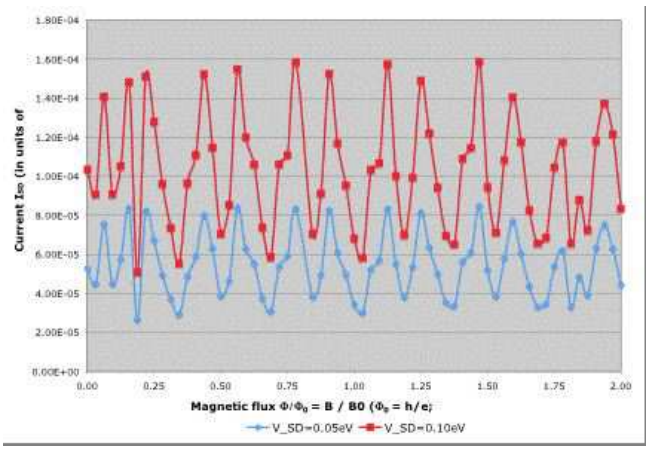

Fig. 4 b.

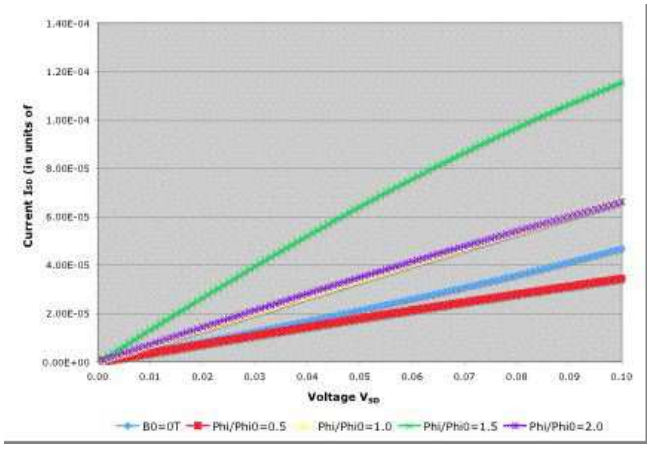

Fig. 4 c.

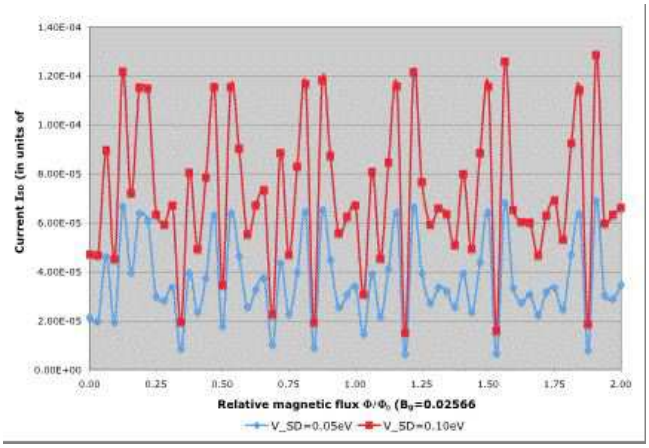

Fig. 4 d.